


# High-Resolution Methods for Diagnosing Cartilage Damage *In Vivo*

Cartilage  
2016, Vol. 7(1) 39–51  
© The Author(s) 2015  
Reprints and permissions:  
sagepub.com/journalsPermissions.nav  
DOI: 10.1177/1947603515602307  
cart.sagepub.com  


Kira D. Novakofski<sup>1</sup>, Sarah L. Pownder<sup>2</sup>, Matthew F. Koff<sup>2</sup>,  
Rebecca M. Williams<sup>3</sup>, Hollis G. Potter<sup>2</sup>, and Lisa A. Fortier<sup>1</sup>

## Abstract

Advances in current clinical modalities, including magnetic resonance imaging and computed tomography, allow for earlier diagnoses of cartilage damage that could mitigate progression to osteoarthritis. However, current imaging modalities do not detect submicrometer damage. Developments in *in vivo* or arthroscopic techniques, including optical coherence tomography, ultrasonography, bioelectricity including streaming potential measurement, noninvasive electroarthrography, and multiphoton microscopy can detect damage at an earlier time point, but they are limited by a lack of penetration and the ability to assess an entire joint. This article reviews current advancements in clinical and developing modalities that can aid in the early diagnosis of cartilage injury and facilitate studies of interventional therapeutics.

## Keywords

cartilage, imaging, MRI, CT, multiphoton microscopy

## Osteoarthritis and Motivation for High-Resolution Cartilage Imaging

Osteoarthritis (OA) is a progressive disease<sup>1,2</sup> initiated at an unknown time before clinical signs are apparent.<sup>3</sup> To attenuate the natural progression of disease, early detection of damaged cartilage is needed. However, current clinical imaging techniques are limited in resolution and likely underdiagnose microscopic cartilage damage.<sup>4,5</sup> With improved detection of cartilage damage, diseased cartilage can be identified earlier which will strengthen the knowledge of the pathogenesis of OA and facilitate development of new treatments.

The 3 commonly used noninvasive clinical modalities are radiography, magnetic resonance imaging (MRI), and computed tomography (CT). Radiographs are often used as a screening method. Radiographs cannot directly visualize the soft tissue of cartilage but instead are used to identify changes in subchondral bone. It might not be possible to detect secondary bone changes radiographically within a year of injury.<sup>6</sup> MRI and CT can diagnose changes within the cartilage matrix. Traditional MRI and CT are thought to more likely underdiagnose than overdiagnose cartilage defects,<sup>4,5</sup> although current quantitative techniques offer more sensitive methods for detection of early matrix depletion. *In vivo* or arthroscopic imaging techniques often have higher resolution than MRI or CT and can provide biological information, but they are invasive and require direct visualization of the articular surface. Arthroscopic *in vivo* imaging

techniques include optical coherence tomography (OCT), ultrasonography, bioelectricity including streaming potential measurement, and multiphoton microscopy (MPM) (Table 1). All of these techniques provide highly detailed information about cartilage structure (Fig. 1).<sup>7</sup>

## Magnetic Resonance Imaging

Magnetic resonance imaging is performed using nonionizing radiation to excite MRI-suitable nuclei, of which hydrogen protons are most commonly used due to their copious concentration in soft tissue. When placed in a strong magnetic field, protons precess parallel or antiparallel to the main magnetic field ( $B_0$ ). More protons are aligned parallel to  $B_0$ , creating a net magnetic vector in the direction of  $B_0$ . Application of a pulse of specific radiofrequency (RF) rotates the net vector from the main magnetic field into the transverse plane. When protons precess in this perpendicular plane, a current is induced in a receiver coil around the anatomy of interest, which is converted to voltage and used

<sup>1</sup>Department of Clinical Sciences, Cornell University, Ithaca, NY, USA

<sup>2</sup>MRI Laboratory, Hospital for Special Surgery, New York, NY, USA

<sup>3</sup>Department of Biomedical Engineering, Cornell University, Ithaca, NY, USA

### Corresponding Author:

Lisa A. Fortier, Department of Clinical Sciences, Cornell University, VMC C3-181, Ithaca, NY 14853, USA.  
Email laf4@cornell.edu

**Table 1.** Imaging Techniques.<sup>a</sup>

Technique	Application	Resolution Range	Clinical Use?	Invasive?
Magnetic resonance imaging		13.7 to 540 $\mu\text{m}$ <sup>8,9</sup>		
T1, T2	Collagen content from hydration <sup>10</sup> and orientation <sup>11</sup>		Yes	No
T2*	Collagen from hydration <sup>12</sup>		Limited trials	No
T1 $\rho$	Glycosaminoglycan (GAG) concentration from hydration <sup>10,13,14</sup>		Limited trials	No
dGEMRIC	GAG concentration by dye exclusion <sup>15,16</sup>		Yes	Minimal (injection)
<sup>23</sup> Na	GAG concentration <sup>17,18</sup>		Limited trials	No
Computed tomography				
Contrast (gadopentetate, ioxaglate)	GAG concentration by dye exclusion		Yes	Minimal (injection)
Contrast (anionic)	Measure of GAG concentration		Laboratory	Minimal (injection)
Phase contrast x-ray computed tomography	Matrix inhomogeneity by x-ray scattering <sup>19</sup>	8 $\mu\text{m}$	Laboratory	No
Optical coherence tomography	Matrix inhomogeneity by backscattering of infrared light	10 $\mu\text{m}$ , <sup>20,21</sup> depth limited to 1.5 mm <sup>22</sup>	Yes	Yes
Ultrasonography	Matrix inhomogeneity by sound wave attenuation and refraction	30 $\mu\text{m}$ , <sup>23</sup> depth limited to 1.65 mm <sup>24</sup>	Yes	No, yes (method dependent)
Streaming potential measurement	Indirect GAG inhomogeneity with fluctuations in cationic ions <sup>25,26</sup>	Not applicable	Laboratory	No, yes (method dependent)
Multiphoton microscopy	Cell death and matrix inhomogeneity with excitation by infrared radiation	<1 $\mu\text{m}$ , <sup>27</sup> depth limited to 200 $\mu\text{m}$ <sup>28</sup>	Laboratory	Yes

<sup>a</sup>Magnetic resonance imaging (MRI) and computed tomography (CT), optical coherence tomography (OCT), ultrasonography, electric streaming potential, and multiphoton microscopy (MPM) can be used to acquire data about tissue, which in turn can be used to determine tissue properties. Some of the described methods are currently used clinically, while others are in the process of Food and Drug Administration approval (limited trials), or are still in laboratory development (laboratory). Some methods are noninvasive for the patient, while others require arthroscopy.

to create the MR signal. When the RF pulse is removed, tissue protons immediately lose energy and realign with  $B_0$ . Two concurrent but independent processes occur: longitudinal regrowth associated with spin-lattice relaxation and transverse decay associated with spin-spin relaxation. Spin lattice relaxation involves the process in which tissue protons give up energy to their surrounding environment, and the gradual regrowth of net magnetization vector as a time rate defined as T1. Spin-spin relaxation involves dephasing secondary to local field inhomogeneities. The dephasing results in a decay of signal with a time rate defined as T2 relaxation time. The signal intensity of a given tissue varies with the timing parameters of the RF pulses supplied to tissue protons.

With MRI, the ability to detect cartilage abnormalities depends on a combination of factors including: field strength, coil selection, type of pulse sequence, and MR parameters (field of view [FOV], slice thickness, in-plane spatial resolution). Field strengths common in clinical use are 1.5 T and 3.0 T, while research scanners may be 4.7 T and higher. Higher field strengths can provide increased signal to noise ratio (SNR) for a given pulse sequence, with the advantage of reduced time because fewer acquisitions (NEX, NAQ) are required. Higher field strength magnets

have drawbacks compared to clinical field strength magnets, particularly with increased specific absorption rate (SAR), cost, and fewer coil options which may limit routine clinical use. Chemical shift artifacts are also more pronounced with increasing field strength, and this is important when considering that frequency misregistration of marrow fat may affect imaging of an overlying thin cartilage surface. High field strength magnets have an improved ability to image smaller specimens because increased spatial resolution is possible with increased SNR. However, long scan times and specialty coils with small FOV are often required, thus prohibiting imaging of large specimens at the same resolution. Imaging an intact human joint at 7 T has been reported,<sup>29,30</sup> but the protocols used were similar in spatial resolution to that achievable at 3 T. Future clinical application and development of 7 T proton MRI may ultimately be hindered by commercial availability of scan coils and subsequently, development of protocols. It should be considered, however, that these deterrents were historically present for 3 T MRI, which is now standard of care in many radiology units.

Several pulse sequences have been used for assessment of articular cartilage.<sup>31-37</sup> Fat-suppressed three-dimensional spoiled gradient-recalled sequences are commonly cited;

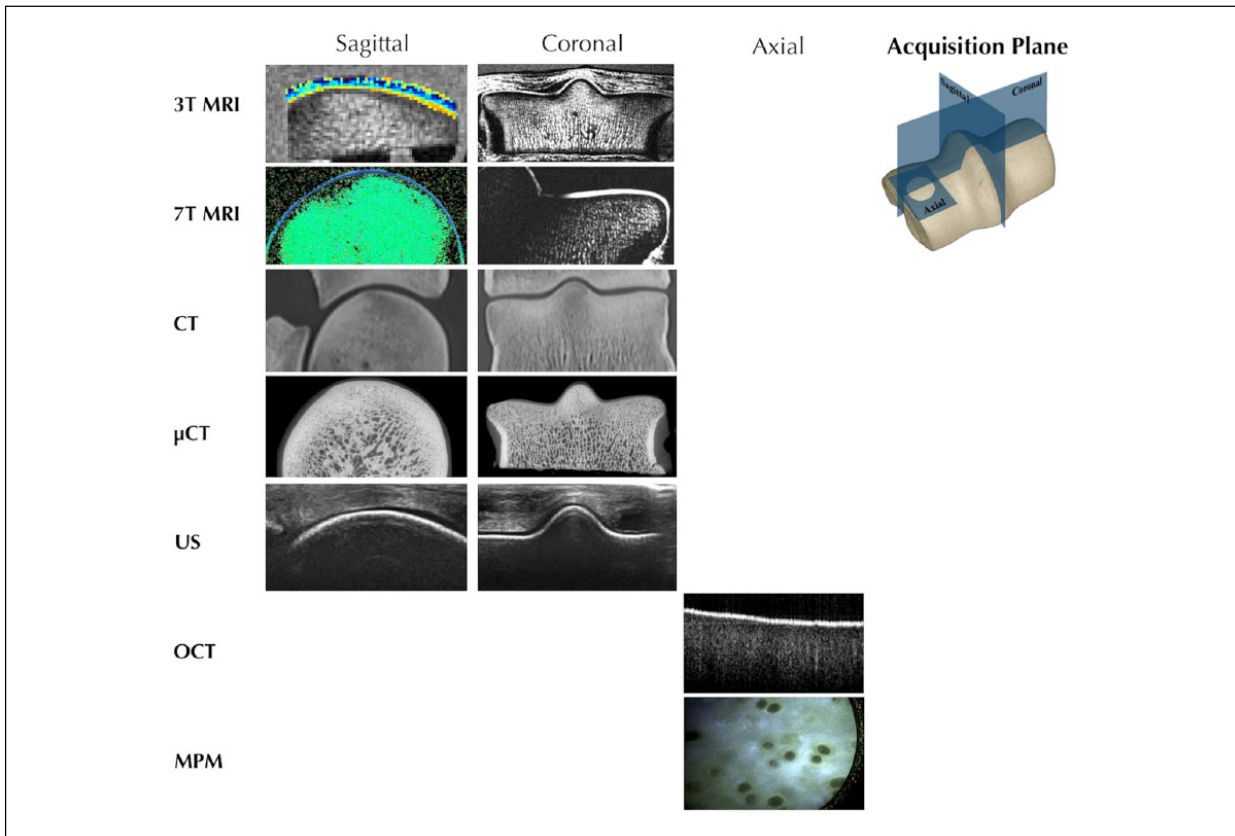


**Figure 1.** Each imaging modality can be used to collect information about the tissue, often in multiple acquisition planes. This information can be combined to provide a comprehensive picture of the tissue. Magnetic resonance imaging (MRI) and computed tomography (CT) provide structural information in sagittal, coronal, and axial (not shown) planes, about full thickness cartilage and subchondral bone. Ultrasonography (US) and optical coherence tomography (OCT) provide information about the structural integrity of cartilage with limited penetration into bone. Multiphoton microscopy (MPM) can be used to acquire axial images with submicron resolution, including the identification of individual cells, but with limited depth penetration from the surface to  $\sim 200$   $\mu\text{m}$ .

however, these sequences tend to have long acquisition times and often lack the soft tissue contrast resolution necessary to assess the remaining joint.<sup>33,34,36</sup> Additionally, certain gradient echo sequences (eg, DESS) have been shown to underdiagnose small focal cartilage defects.<sup>38</sup> Fast spin-echo (FSE) proton density-weighted (PD) images delineate articular cartilage, adjacent synovial fluid, and cortical bone, providing a useful grayscale image dynamic range window in which hyaline articular cartilage can be evaluated without the need for contrast injection.<sup>39</sup> Because of inherent magnetization transfer effects caused by the multiple refocusing pulses and multislice acquisition in FSE sequences, articular cartilage has lower signal intensity than in spin echo (SE) sequences, thereby providing important differential contrast between fluid and cartilage.<sup>37,39-41</sup> The reduced scanning time for equal or greater coverage afforded by FSE imaging over SE imaging further emphasizes its clinical utility. T1-weighted and T2-weighted

imaging, which are used predominantly in neuroimaging, do not provide the tissue contrast necessary to fully assess cartilage.

Articular cartilage on standard of care FSE MRI has a lamellar appearance due to regional cartilage collagen orientation. Proton-proton interactions shorten T2 resulting in a loss of signal in regions of more highly ordered collagen, for example, in the deep zone of cartilage. This signal loss is more pronounced with increasing echo time (TE). The superficial, intermediate, and deep zones represent approximately 5% to 10%, 45%, and 40% to 45% of the depth of cartilage, respectively. The superficial zone collagen fibrils are oriented parallel to the articular surface (producing limited signal), intermediate zone collagen is more randomly oriented (producing greater amounts of signal), and deep zone collagen is radially oriented (producing limited signal). Loss of normal gray-scale stratification is an important clinical feature that may be an indication of subsequent

delamination of cartilage from subchondral bone.<sup>37</sup> Additionally, MRI quantification of cartilage thickness may serve as marker of OA and is more sensitive than radiographs in identifying changes in joint space width.<sup>42</sup> These changes are associated with early OA but are not reliably detected on standard of care MRI,<sup>39</sup> most likely because biochemical matrix changes precede structural matrix changes. Use of intravascular or intra-articular contrast agents is common; however, noncontrast MRI techniques identify tears in labral cartilage with accuracy similar to MR arthrography and better than previously reported.<sup>43</sup> The added discomfort of an intra-articular injection as well as potential side effects of contrast agents should also be considered when selecting arthrography.

Quantitative magnetic resonance imaging (qMRI), including T2 mapping, delayed gadolinium-enhanced MRI of cartilage (dGEMRIC), and T1 rho (T1 $\rho$ ) are useful diagnostic tools for assessing articular cartilage because they objectively evaluate the biochemical properties of tissue.<sup>44-50</sup> These are useful pulse sequences because they can detect biochemical changes that precede morphological degeneration in tissue and may help hasten early diagnosis and treatment of OA.

### T2-Mapping

T2-mapping is a commercial product from many vendors and works by acquiring images at multiple echo times. The transverse decay constant, T2, is calculated on a pixel-by-pixel basis by fitting the signal intensity as a function of time using a negative exponential curve. T2 relaxation times represent the decay of transverse magnetization due to loss of phase coherence after removal of an RF pulse.<sup>51,52</sup> T2 decay is strongly influenced by free water molecules, which slow the loss of transverse magnetization and results in prolongation of T2 values.<sup>52</sup> T2-mapping has been used for measuring increased water content and loss of collagen orientation OA with resultant prolonged T2 values.<sup>53,54</sup> The sensitivity of T2 mapping for detection of changes in collagen orientation has been shown in *ex vivo* tissue and live specimens.<sup>53,55</sup> Although initially thought to not be associated with proteoglycan content, new evidence suggests negatively charged glycosaminoglycans (GAGs) influence the interaction of water protons.<sup>52</sup> T2 relaxation times vary with age; children with open physes demonstrate prolonged T2 compared with individuals with closed physes.<sup>56</sup> In addition, asymptomatic adult volunteers have demonstrated a gradual increase of T2 in aging cartilage.<sup>57</sup> T2 values also vary with region, coil selection, and species.<sup>58,59</sup>

### dGEMRIC

dGEMRIC provides an inverse relationship of GAG concentration with use of the negatively charged contrast agent

gadolinium diethylenetriaminepentacetate (Gd-DTPA<sup>2-</sup>; gadopentetate).<sup>15</sup> dGEMRIC has been shown to be reproducible (intraclass correlation 0.87-0.95) when reimaging the same knee in early OA.<sup>16</sup> T1 relaxation time in the presence of Gd-DTPA<sup>2-</sup> is approximately linearly related to the GAG content of cartilage through assessment of fixed charge density.<sup>52,53</sup> Previous investigators have estimated the concentration of contrast agent in cartilage from T1 values using the dGEMRIC protocol.<sup>52</sup> The dGEMRIC protocol detects reduced proteoglycan content in cartilage during the early stages of OA. However, it is slightly invasive necessitating a contrast injection, delayed imaging is needed (90-120 minutes for most joints), and low level exercise is recommended following administration of contrast. Combined, this typically adds an additional 1.5 to 2 hours to the scanning protocol.

### T1 $\rho$

T1 $\rho$  is spin lattice relaxation in the rotating frame and is sensitive to low-frequency interactions between water and the local macromolecular environment; more specifically, the proteoglycan constituents of the extracellular matrix (ECM) in cartilage.<sup>60</sup> T1 $\rho$  and fixed charged density are strongly correlated ( $R^2 > 0.75-0.85$ )<sup>60</sup> and fixed charge density is a reflection of proteoglycan content. T1 $\rho$  in cartilage is associated with relaxation of water protons in the presence of macromolecular components, such as proteoglycans, in the ECM. Therefore, loss of proteoglycans in the ECM are reflected as prolongation in T1 $\rho$  relaxation time.<sup>60</sup> Because proteoglycan content typically decreases prior to structural changes in collagen, this may serve as a sensitive indicator for early OA. T1 $\rho$  is an attractive alternative to dGEMRIC because it does not require injection of a contrast agent, exercise, or delayed scanning to evaluate proteoglycans.

Differences in T1 $\rho$  and T2-mapping between cartilage of normal individuals and those with arthroscopically or histologically confirmed OA have been reported, and the reproducibility of these methods continues to be evaluated.<sup>58,61</sup> Sources of variation that affect T2-mapping include scanner and coil type, magnet strength, patient and control populations, imaging protocol, T2-mapping sequence parameters, post-image processing, method of calculation, and analysis/reporting of values.<sup>58</sup> It has been suggested that T1 $\rho$  is superior to T2 mapping for evaluation of mild OA. Both T1 $\rho$  and T2 mapping discriminate between mild and moderate or moderate and severe OA; however, T1 $\rho$  can differentiate normal and mild OA while T2-mapping cannot.<sup>62</sup> This might be anticipated because during the beginning stages of OA, the collagenous component of the ECM is often preserved while proteoglycan loss is characteristic of early OA. Few studies have concurrently compared all three quantitative techniques. One study of young anterior

cruciate ligament-injured patients found no appreciable focal GAG loss detected by dGEMRIC or general elevation of T2, but general and focal T1 $\rho$  relaxation times were increased, indicating an acute increase in unbound water in the matrix after blunt trauma.<sup>63</sup> Of note, both T1 $\rho$  and T2 can predict cartilage loss in subjects with no or mild radiographic OA over a two-year period.<sup>64</sup>

### Sodium MRI

Sodium MRI provides a highly specific measure of sodium concentration in a tissue. Sodium is a positive counter ion to the negatively charged GAG side chains of proteoglycans. Sodium imaging provides a specific measure of proteoglycan content.<sup>60</sup> Sodium MRI has a high correlation with GAG concentration; however, acquisition times are typically long (>15 minutes), images have reduced SNR compared with proton MRI, and specialized multinuclear coils are required for imaging <sup>23</sup>Na. Techniques including compressed sensing by undersampling k-space have been investigated to shorten scan duration.<sup>65</sup> Sodium MRI at 7 T has been used to detect early cartilage degradation by measuring the change in concentration of <sup>23</sup>Na associated with GAG loss.<sup>65</sup> Sodium MRI may be a tool for diagnosing early cartilage degeneration, but this MRI technique still needs further development to provide better resolution and faster scan times before being feasible for routine clinical use.

### GAG-CEST

Chemical exchange-dependent saturation transfer (CEST) MRI allows quantification of macromolecules by measuring chemical exchanges between side chains of large macromolecules with those of the “free” water or bulk water pool.<sup>66</sup> In GAG-CEST, side chains of GAG macromolecules, specifically the GAG hydroxyl (–OH) protons, are presaturated with a selective RF pulse, and a chemical exchange of these protons with free water protons occurs. Differences between the presaturated and unsaturated images are compared to assess the signal from GAG molecules. The exchange of protons results in a detectable decrease in magnetization of the bulk water pool.<sup>67</sup> A benefit of GAG-CEST is increased sensitivity to a relatively low concentration of GAG molecules due to the abundance of bulk water. This imaging technique is attractive as it opens the possibility of measuring GAG concentrations *in vivo* with clinically feasible scan times of approximately 5 minutes.<sup>68</sup> However, GAG-CEST is sensitive to fluctuations in B<sub>0</sub>; therefore, requiring a correction for the local B<sub>0</sub> variation.<sup>69</sup> Furthermore, less chemical exchange effect is noted at the more ubiquitously utilized field strengths of 3 T due to direct saturation effects and a fast exchange rate. For this reason, some investigators have limited its application to 7 T imaging.

### Diffusion Techniques

Diffusion-weighted imaging (DWI) is commonly used in neuroimaging for detection of early ischemia. DWI incorporates a pair of gradients with opposite polarity, resulting in attenuation of signal due to dispersion of spins. The amount of signal reduction is proportional to the amount of diffusion in the tissue and can be measured as an apparent diffusion coefficient (ADC).<sup>70</sup> Performing repeated diffusion measurements and changing the direction of the diffusion-encoding gradient permits performance of diffusion tensor imaging (DTI) and calculation of the diffusion tensor. The diffusion tensor represents the diffusion at an individual voxel in three-dimensional space. The principal values (eigenvalues) and principal directions (eigenvectors) of the diffusion tensor indicate apparent diffusivities and their associated directions along the axis of principle diffusion.<sup>71</sup> The principal values can be used to calculate mean diffusivity, the degree to which proton motion is permitted due to the local environment, and to calculate fractional anisotropy, the effect local tissue orientation has on the preferred direction of diffusivity.

Diffusion-weighted/DT imaging in cartilage has been proposed due to the high water content, the local preferred orientation of collagen fibrils, and the changes in permeability and organization during the onset and progression of OA. Previous studies have shown elevated levels of the apparent diffusion coefficient<sup>72</sup> and reduced fractional anisotropy in cartilage with structural changes associated with OA.<sup>73</sup> The challenges of *in vivo* diffusion quantitation of cartilage include the relatively short T2 values of cartilage, the voxel resolution required for evaluation,<sup>74</sup> and the sensitivity of pulse sequences to joint motion (owing to the necessity of multidirectional diffusion measurements).<sup>75</sup>

### Computed Tomography

Computed tomographic imaging works by rotating a narrow beam of x-rays around a patient or tissue sample. Once the beam passes through the patient or tissue of interest, specialized detectors receive the attenuated x-ray beam, and a computer converts the information into cross-sectional images or slices. Multiple image slices and three-dimensional reconstructions are created by computer processing, which yield detailed information about deep tissue, eliminating the superimposition of structures that is seen with conventional radiography. CT provides some soft tissue contrast resolution because some tissue types can be differentiated by measurement of Hounsfield units (HU). Newer dual energy scanners provide improved soft tissue contrast. Intra-articular structures are often assessed in the setting of intra-articular or intravenous contrast agents to provide additional soft tissue resolution. Using soft tissue kernel-based CT with postprocessing, CT can identify

regions of different cartilage thickness in the human shoulder, with results similar to MRI or anatomical sections.<sup>76</sup> However, fine details of cartilage needed to identify early OA are not easily visualized with standard soft tissue CT imaging. Contrast agents and acquisition methods have made it possible to achieve cartilage details that correlate with MRI.<sup>77</sup>

Contrast agents commonly used during CT imaging are typically anionic, iodine-based. Contrast agents are either excluded from or are attracted to the cartilage matrix. Negatively charged GAGs repel anionic agents and attract cationic agents. Imaging with anionic contrast agents is achieved because anionic agents are concentrated in regions with little GAG such as the synovial fluid or cartilage lesions, or alternatively, by being excluded from regions that are dense with GAGs such as normal cartilage. Healthy cartilage will have less anionic contrast present than diseased cartilage that is depleted of GAGs. CT scanning with anionic, iodine-based contrast agents has been reported to both highly correlate (anionic tri-iodinated agent,  $R^2 = 0.83$ )<sup>78</sup> and poorly correlate (ioxaglate,  $R^2 = 0.2$ ,<sup>79</sup>  $R = -0.64$ )<sup>80</sup> with biochemically measured GAG content by dimethylmethylene blue (DMMB) assay<sup>78,79</sup> or safranin-O staining.<sup>80</sup> Different types of anionic iodinated agents, levels of degradation, and lengths of dye incubation can contribute to differing results of CT imaging. Optimizing methods for *in vivo* incubation may improve GAG correlation, and subsequently, clinical diagnosis. Ioxaglate can detect small cartilage injuries in as little as 3 hours after trauma.<sup>81</sup> However, anionic agents take more than 29 hours for diffusion to reach near-equilibrium state.<sup>82</sup> Cartilage injury can be detected in almost a tenth of the time needed for contrast to reach the diffusion equilibrium within cartilage, but the accuracy of quantifying the severity of injury may be limited with a 3 hour incubation. In addition, some contrast agents such as ioxaglate do not cross the bone-cartilage interface,<sup>80</sup> suggesting that intra-articular injection may be more effective than intravenous injection.

Cationic contrast agents provide a solution to the limitations of anionic agents. Cationic agents like CA4+ have a higher correlation with GAG ( $R^2 = 0.83$ ) than negatively charged agents (ioxaglate  $R^2 = 0.2$ ; gadopentetate  $R^2 = 0.22$ ).<sup>79</sup> Further development is necessary to help achieve detailed imaging of cartilage with anionic and cationic agents that have high correlations to matrix biochemical properties.

Cartilage can also be imaged using CT without contrast agents with new acquisition methods. Normal and arthritic human patellar cartilage can be identified with phase contrast (PCI) x-ray CT (PCI-CT). In PCI-CT, a highly collimated x-ray beam is delivered to the sample, and emerging, refracted, or scattered radiation is enhanced with respect to the ballistic radiation. Collected light is analyzed to determine an apparent "pattern" or "texture" of the matrix. While this method is being tested with *ex vivo* samples, it may

have a future role with adaptation for detecting small matrix defects, with its high resolution of  $8 \mu\text{m} \times 8 \mu\text{m}$  per pixel.<sup>19</sup> Use of a highly collimated x-ray beam in a synchrotron facility would need to be adapted for clinical application.

Resolution of CT can be achieved at the submicron level.  $\mu\text{CT}$  can provide higher resolution imaging for *ex vivo* samples or *in vivo* imaging of small specimens similar to that of a small rodent. Standard  $\mu\text{CT}$  has a resolution of 25 to 85  $\mu\text{m}^3$  voxels, although some  $\mu\text{CT}$  systems having the capability of submicron resolution as described above.<sup>19,79,83</sup> However, contrast dyes are still required to visualize cartilage in  $\mu\text{CT}$ . In addition, the safety of  $\mu\text{CT}$  for patients needs to be further evaluated, but equipment and acquisition modifications could reduce  $\mu\text{CT}$  radiation exposure to similar levels of current clinical CT.<sup>84</sup> While iterative reconstruction algorithms reduce the burden of ionizing radiation, it is not eliminated. In addition, the overall soft tissue contrast is inferior to MRI and most investigators focus on the use of MRI to assess cartilage morphology and structure.

## Optical Coherence Tomography

Optical coherence tomography (OCT) provides a cross-sectional view of cartilage from an arthroscopic or open-joint approach. This imaging technique collects backscattered infrared light, providing deep penetration of tissue to reveal subsurface defects.<sup>85</sup> Using OCT, the integrity of ECM collagen matrix can be assessed, thickness of cartilage can be measured, and bone-cartilage interface can be evaluated.

A handheld OCT probe<sup>86</sup> can be inserted arthroscopically through a  $\leq 0.9$  mm portal.<sup>20</sup> OCT has an in-plane resolution of about  $10 \mu\text{m}$ <sup>20,21</sup> and depth penetration of up to 1.5 mm.<sup>22</sup> Cartilage thinning and fibrillation as well as birefringence of collagen can be visualized. Modified Mankin scoring of OCT optical sections and histological slide sections have high agreement ( $\kappa = 0.80$ ),<sup>85</sup> suggesting that OCT can serve as an effective method to assess deeper tissue that cannot be seen with an arthroscopic lens. OCT signal intensity and edge variance correlates with  $313 \mu\text{m} \times 313 \mu\text{m}$  resolution, T2-mapping in MRI.<sup>22</sup>

Using various evaluation methods, including International Cartilage Repair Society (ICRS) lesion scoring parameters,<sup>20</sup> OCT roughness index (ORI),<sup>87,88</sup> optical surface reflection coefficient (ORC),<sup>87,88</sup> variation of surface reflection (VSR),<sup>88</sup> and optical backscattering (OBS),<sup>88</sup> cartilage degradation can be quantified. ICRS scoring with OCT can provide an overall assessment of cartilage disease but has only moderate correlation with standard arthroscopy ( $R = 0.503$ ).<sup>20</sup> ORI, ORC, VSR, and OBS can be used to detect cartilage injury caused by mechanical trauma.<sup>88</sup> ORI and ORC decrease in bovine cartilage treated with collagenase but not trypsin, suggesting OCT may be more sensitive to changes in collagen than GAG.<sup>87</sup> This is not surprising because OCT relies on reflection, and collagen fibrils are reflective, unlike GAGs.

Optical coherence tomography has the resolution to differentiate cartilage zones due to the different refractive indices (RI) among zones.<sup>89</sup> However, different RIs have been reported between species in the literature,<sup>89,90</sup> which can affect cartilage depth measurements. This suggests that optimization of imaging parameters may need to be outlined prior to evaluating cartilage. Furthermore, when acquiring OCT images, if the probe is not perpendicular to the surface, ORI, ORC, VSR, and OBS can be affected.<sup>88</sup> OCT has an in-plane resolution of about 10  $\mu\text{m}$ , which is about the size of one cell, but it cannot discern cellular viability or morphology.

## Ultrasonography

Ultrasonography uses non-ionizing sound waves to create real-time images. Medical ultrasound machines generate and receive sound waves greater than 20,000 Hz using specialized probes or transducers consisting of piezoelectric elements that convert electrical energy into sound and vice versa. The generated sound waves travel from the transducer surface and penetrate tissue to variable degrees based on wave frequency and tissue composition. Sound waves may be reflected, transmitted, refracted, or absorbed during interaction with tissue. Reflected echoes include specular reflections from smooth, broad boundaries, while scattered nonspecular reflections occur when the reflective interface is smaller than the sound wavelength of the applied ultrasound beam. Small nonspecular reflectors give each tissue a characteristic scatter signature. Returning sound waves are received at the transducer surface, translated into an electric current, and analyzed based on signal amplitude and acquisition time. This results in a composite image representative of a tissue in cross section with depth and width determined by the transducer configuration.

Ultrasound probes vary in configuration of piezoelectric elements, shape of the image plane, manner in which the beam is focused, and size of the transducer footprint. The size and shape of the transducer are fixed but must be considered, particularly when assessing a convex surface with a convex probe, in which the perpendicular angle of insonation will be represented by a very small portion of the image field. Lower frequency probes provide improved depth penetration at the expense of spatial resolution, while higher frequency probes afford a greater spatial resolution at the expense of depth penetration. It is important to match probe selection to the region and tissue of interest.

Ultrasound machines for transdermal use are portable, noninvasive, and can be housed in an office setting. Collagen strongly scatters ultrasound signals in soft tissues<sup>91-94</sup> due to mismatch in acoustic impedance of collagen and surrounding soft tissue. Chondrocytes are approximately 10  $\mu\text{m}$  in diameter and appear to act as an additional source of scatter.<sup>95</sup> Cartilage can be imaged through skin but not bone.

Intra-articular ultrasonography techniques have been developed to image highly concealed regions by introducing intravenous ultrasound probes through arthroscopic ports. Although intra-articular ultrasonography requires a camera to determine probe location, it has been suggested that a vascular probe could be introduced into the joint through a small needle and that the three-dimensional position of the probe could be monitored externally and separately with a second probe.<sup>96</sup> Conventional ultrasonography does not provide sufficient resolution to visualize microscopic details of cartilage structure.<sup>97</sup> The use of higher frequency probes, up to 50 MHz penetrate the subsurface structure of cartilage and permit detection of additional information from articular cartilage, including backscatter patterns that are undetectable using clinical probes.<sup>97</sup> Although higher frequency transducers are available to provide greater spatial resolution, ultrasound microscopy using transducers of 60, 80, and 100 MHz fail to adequately penetrate juvenile porcine cartilage, which is on the order of 4 mm.<sup>97</sup> Therefore, the highest frequency probe with adequate depth penetration should be selected to assess a given region of interest. Another consideration for the use of intra-articular ultrasonography is the surface area covered by an individual image. Ultrasound beam diameter of intravascular probes is approximately  $1 \times 4$  or  $2.8 \times 4$  mm<sup>97-99</sup> and would require hundreds or thousands of images in order to assess the whole joint. Such applications may be best suited for regions of interest such as repair sites.

## Quantitative Techniques

Several quantitative techniques have been developed to evaluate cartilage on the articular surface, within the ECM, and at the cartilage-subchondral bone interface. Four measures are most commonly utilized: ultrasound roughness index (URI), ultrasound reflection coefficient (R), integrated reflection coefficient (IRC), and apparent integrated backscattering (AIB). These parameters assess surface continuity of the articular margin, the reflective characteristics of the superficial and deep margins of cartilage, and the inherent scatter signature of cartilage architecture.

The URI is based on a measurement of ultrasound flight time between the transducer and cartilage surface.<sup>98</sup> It is not as dependent on the angle of insonation as are the other quantitative parameters and may have greater clinical utility when imaging curved articular surfaces. URI has lower reliability with lower frequency transducers, including 5 and 10 MHz,<sup>100</sup> which results in the recommended use of higher (30-50 MHz) transducers. URI calculations of mechanically damaged, enzymatically degraded, and naturally degenerated cartilage reveal elevations in damaged/diseased samples compared with intact, health cartilage.<sup>98,101-105</sup> The URI correlates with surface irregularity seen with surface fibrillation in the early stages of OA.

Reflection coefficient  $R$  and IRC are both typically measured at the joint-cartilage interface and at the cartilage-subchondral bone interface to assess specular reflective properties.  $R$  is the proportion of the ultrasound pulse reflected at the cartilage surface determined in the time domain. IRC is similarly determined but in the frequency domain.  $R$  and IRC decrease at the cartilage surface in mechanically or enzymatically degraded cartilage<sup>93,98,101-105</sup> but increase at the cartilage-bone interface due to higher acoustic impedance in sclerotic subchondral bone.<sup>106</sup>

Apparent integrated backscattering measures the scattering properties of cartilage matrix. The source of backscatter is a result of both chondrocyte density and collagen concentration.<sup>95</sup> Backscatter is a measure of the inherent scattering or small reflective surfaces in the tissue and increases with increasing collagen content and chondrocyte concentration. There is inherent loss of backscatter proportional to the depth of tissue due to inherent attenuation of the ultrasound beam at higher frequencies and must be corrected for accurate assessment.<sup>98</sup> In degenerative conditions, AIB decreases due to loss of inherent scatter.

Ultrasound elastography has been used as a method of evaluating the stiffness of soft tissues, particularly abdominal tissues in which neoplastic or global organ diseases alter composition and increased stiffness. Elastography may be an ideal tool to assess loss of stiffness in tissues such as diseased or damaged cartilage. As cartilage is stiffer than most visceral soft tissues previously examined with elastography, the output intensity needed may exceed the current predefined safety thresholds.<sup>107</sup> Research in this area is ongoing

## Bioelectricity

Cartilage degeneration can be evaluated by capitalizing on its bioelectrical properties. Streaming potential due to positively-charged sodium ions and negatively-charged GAGs<sup>25,26</sup> or bulk electrical impedance due to water content<sup>108</sup> can be used to assess the integrity of cartilage, which can be graded with both noninvasive external methods and *in vivo* methods. By loading and unloading the knee, fluid flow generates a flux of sodium ions, which creates a streaming potential that can be measured both noninvasively and *in vivo*. Streaming potential can be detected with electroarthrography (EAG), where electrodes are placed on the skin near the joint line.<sup>26</sup> Significantly different streaming potentials can be detected between normal and OA knees using EAG. However, repeatability of measurements within a normal knee is site dependent, with some sites closer to the joint line being more consistent than those farther from the joint line.<sup>26</sup> Site dependency could affect results when evaluating a joint for disease, particularly if the test is performed by different clinicians. The possibility of diagnosing OA with noninvasive streaming potential by EAG is promising, particularly among other

developing cartilage techniques that require invasive procedures. EAG may be effective for initial OA screening as a diagnostic tool, but the relatively low resolution of EAG makes it inappropriate for fine-tuned diagnostics.

Electrical streaming potential can also be measured arthroscopically. Measurements of electrical streaming potential *in vitro* and *in vivo* are sensitive and can detect changes in the ECM after enzymatic degradation,<sup>109</sup> or mechanical injury.<sup>110</sup> A streaming potential integral (SPI) can be measured by indenting the cartilage surface with an arthroscopically designed probe. SPI has been shown to correlate with ICRS and Mankin scores ( $R = -0.749$  and  $-0.409$ , respectively).<sup>111</sup> SPI measurements are significantly different between normal cartilage and moderately to severely mechanically injured cartilage resulting from 28- to 49-MPa loading.<sup>110</sup> The logarithm of SPI also correlates with cartilage thickness ( $R = -0.496$ ), suggesting that it may be applied clinically to determine differences in site-to-site cartilage-bone interfaces.<sup>111</sup> SPI has a high intraclass correlation between repeated measurements by different users (ICC = 0.861).<sup>110</sup> However, the sensitivity of SPI is limited, and it fails to detect a significant difference between normal cartilage and mild injuries created by 17-MPa loading.<sup>110</sup> SPI might compliment arthroscopic examination by providing details of deeper cartilage but could be limited in the additional information it can provide. By improving the sensitivity of *in vivo* SPI measurement, this high inter- and intrauser repeatable technique could be a promising tool to compliment current arthroscopic imaging.

Electrical impedance, a characteristic of the bulk electrical property of cartilage, can be measured *ex vivo* to detect degraded cartilage. Unlike streaming potential which is dependent on local cartilage properties, electrical impedance is dependent on the bulk of the tissue. In an *ex vivo* setting, a cartilage explant is placed between 2 electrodes, and a voltage is applied to measure impedance. Impedance in cartilage is dependent on the permeability of cartilage to water, which changes when cartilage is degraded. The electrical resistivity significantly decreases after hyaluronidase or collagenase treatment, and the amplitude of change is dependent on the duration of treatment with enzymes.<sup>108</sup> This concept has potential to be used in a clinical setting to diagnose altered matrix integrity.

## Multiphoton Microscopy

Cartilage damage can be visualized at the cellular level using MPM.<sup>112,113</sup> MPM is a microscopic technique that uses pulsed, infrared photons to acquire submicrometer<sup>27</sup> images of intact, live tissue to approximately 200 micrometers in  $z$ -depth.<sup>28</sup> MPM images are gathered by utilizing both the backscattering of excitation photons in the nonlinear optical process called second harmonic generation (SHG) and the 2-photon excitation of both intrinsic autofluorescent



molecules within tissue and exogenous fluorescent dyes added to tissue. MPM images can be acquired from intact and unstained tissue, providing cellular resolution with a penetration that is not available with other microscopic, *in vivo*, or noninvasive imaging techniques.

Cartilage ECM can be visualized with both SHG and autofluorescence. Collagen has strong SHG emission,<sup>114</sup> which can be used to identify and quantify cartilage damage. Quantification of SHG detects differences in collagen content between normal and repair cartilage and correlates with polarized light microscopy ( $R = -0.76$ ).<sup>113</sup> When cartilage is subjected to freezing, which creates structural changes in collagen, SHG intensities diminish.<sup>115</sup> Unlike immuno-staining and polarized light microscopy techniques that require sample processing, SHG with MPM can be used to evaluate matrix collagen in live, intact cartilage samples. Cartilage matrix also contains molecules like elastin<sup>116</sup> that autofluoresce to provide information about extracellular and pericellular matrix.<sup>27</sup> Individual elastin fibers, elastin fiber branching, and diffuse pericellular elastin can be resolved with MPM.<sup>116</sup> Fine details of the ECM can be evaluated when SHG and autofluorescence are combined, including cracks as small as 2  $\mu\text{m}$  that result from mechanical trauma.<sup>112</sup> This type of small damage is undetectable with other *in vivo* imaging techniques.

Multiphoton microscopy can resolve damaged regions of cartilage through the use of dead cell stains<sup>112</sup> and evaluation of matrix diffusivity which is the diffusion and flow of molecules in cartilage.<sup>117</sup> Individual cells can be identified to determine specific regions of increased cell death, such as near matrix cracks that are below the resolution of previously discussed imaging techniques and should aid in the detection of subtle cartilage disease.<sup>112</sup> MPM has not been used clinically to evaluate cartilage, but recent work in other medical fields<sup>118-121</sup> and in *ex vivo* studies<sup>115,117</sup> suggests that MPM has potential as a diagnostic tool. MPM imaging is being investigated in oncology because it can resolve differences between normal and cancerous skin and lung tissues.<sup>118-121</sup> The potential of MPM in the medical field is being realized not only because it can detect differences between normal and abnormal tissue but importantly that it can do so particularly in early stage disease, before abnormalities are detectable with other imaging modalities. MPM can be used to identify small regions of injury in cartilage in an *ex vivo* setting<sup>112</sup> but will require adaptation to a mobile platform before it can be used clinically. With clinical adaptation, subtle cartilage damage can be detected to aid in early diagnosis, treatment, and mitigation of post-traumatic osteoarthritis (PTOA). High-resolution evaluation of cartilage in longitudinal could be performed with arthroscopic MPM to help determine the minimal threshold of damage that degenerates into PTOA and evaluate corresponding therapeutic targets.

## Summary

High-resolution imaging allows early diagnosis of cartilage injury and disease. Identifying and understanding changes in cartilage immediately after injury will benefit patients both directly in the clinic and indirectly through advancement of OA treatments. The superior soft tissue contrast of MRI is ideal for evaluation of cartilage morphology and permits three-dimensional modeling and parametric mapping techniques to enable early assessment of matrix depletion. CT with contrast agents provides excellent spatial resolution but has the disadvantage of ionizing radiation burden. Although OCT, ultrasound, and electric streaming potential have higher resolution compared with clinical MRI and CT, they do not have the submicron resolution or cellular detail that MPM provides. Bioelectricity, OCT, and MPM are promising techniques, but they are all somewhat invasive and would most likely be used as part of an arthroscopic procedure in complement to MRI imaging. The continued development of imaging techniques has the potential for diagnosing early damage, enabling treatment strategies to mitigate the progression to OA.

## Acknowledgments and Funding

This investigation was supported by the Harry M. Zweig Foundation for Equine Research (LAF) and grant TL1RR000459 of the Clinical and Translational Science Center at Weill Cornell Medical College (KDN).

## Declaration of Conflicting Interests

The author(s) declared no potential conflicts of interest with respect to the research, authorship, and/or publication of this article.

## Ethical Approval

This study was approved by our Institutional Animal Care and Use Committee.

## References

1. Felson DT, Lawrence RC, Dieppe PA, Hirsch R, Helmick CG, Jordan JM, et al. Osteoarthritis: new insights. Part 1: the disease and its risk factors. *Ann Intern Med.* 2000;133:635-46.
2. Woolf AD, Pfleger B. Burden of major musculoskeletal conditions. *Bull World Health Organ.* 2003;81:646-56.
3. Gelber AC, Hochberg MC, Mead LA, Wang NY, Wigley FM, Klag MJ. Joint injury in young adults and risk for subsequent knee and hip osteoarthritis. *Ann Intern Med.* 2000;133:321-8.
4. Van Dyck P, Kenis C, Lambrecht V, Wouters K, Vanhoenacker FMHM, Gielen JL, et al. Direct comparison of MR imaging at 1.5- and 3.0-T for evaluating the articular cartilage of the knee. *Insights Imaging.* 2013;4 (1 suppl):S255.
5. Harris JD, Brophy RH, Jia G, Price B, Knopp M, Siston RA, et al. Sensitivity of magnetic resonance imaging for

- detection of patellofemoral articular cartilage defects. *Arthroscopy*. 2012;28:1728-37.
6. Rickey EJ, Cruz AM, Trout DR, McEwen BJ, Hurtig MB. Evaluation of experimental impact injury for inducing post-traumatic osteoarthritis in the metacarpophalangeal joints of horses. *Am J Vet Res*. 2012;73:1540-52.
  7. Arokoski JP, Hyttinen MM, Lapveteläinen T, Takács P, Kosztáczky B, Módis L, *et al*. Decreased birefringence of the superficial zone collagen network in the canine knee (stifle) articular cartilage after long distance running training, detected by quantitative polarised light microscopy. *Ann Rheum Dis*. 1996;55:253-64.
  8. Xia Y, Moody JB, Alhadlaq H. Orientational dependence of T2 relaxation in articular cartilage: a microscopic MRI (microMRI) study. *Magn Reson Med*. 2002;48:460-9.
  9. Souza RB, Kumar D, Calixto N, Singh J, Schooler J, Subburaj K, *et al*. Response of knee cartilage T1ρ and T2 relaxation times to in vivo mechanical loading in individuals with and without knee osteoarthritis. *Osteoarthritis Cartilage*. 2014;22:1367-76.
  10. Duvvuri U, Reddy R, Patel SD, Kaufman JH, Kneeland JB, Leigh JS. T1ρ-relaxation in articular cartilage: effects of enzymatic degradation. *Magn Reson Med*. 1997;38:863-7.
  11. Nieminen MT, Rieppo J, Töyräs J, Hakumäki JM, Silvennoinen J, Hyttinen MM, *et al*. T2 relaxation reveals spatial collagen architecture in articular cartilage: a comparative quantitative MRI and polarized light microscopic study. *Magn Reson Med*. 2001;46:487-93.
  12. Mamisch TC, Hughes T, Mosher TJ, Mueller C, Trattnig S, Boesch C, *et al*. T2 star relaxation times for assessment of articular cartilage at 3 T: a feasibility study. *Skeletal Radiol*. 2012;41:287-92.
  13. Borthakur A, Mellon E, Niyogi S, Witschey W, Kneeland JB, Reddy R. Sodium and T1ρ MRI for molecular and diagnostic imaging of articular cartilage. *NMR Biomed*. 2006;19:781-821.
  14. Jones EF, Schooler J, Miller DC, Drake CR, Wahnische H, Siddiqui S, *et al*. Characterization of human osteoarthritic cartilage using optical and magnetic resonance imaging. *Mol Imaging Biol*. 2012;14:32-9.
  15. Williams A, Gillis A, McKenzie C, Po B, Sharma L, Micheli L, *et al*. Glycosaminoglycan distribution in cartilage as determined by delayed gadolinium-enhanced MRI of cartilage (dGEMRIC): potential clinical applications. *AJR Am J Roentgenol*. 2004;182:167-72.
  16. van Tiel J, Bron EE, Tiderius CJ, Bos PK, Reijman M, Klein S, *et al*. Reproducibility of 3D delayed gadolinium enhanced MRI of cartilage (dGEMRIC) of the knee at 3.0 T in patients with early stage osteoarthritis. *Eur Radiol*. 2013;23:496-504.
  17. Wheaton AJ, Borthakur A, Shapiro EM, Regatte RR, Akella SV, Kneeland JB, *et al*. Proteoglycan loss in human knee cartilage: quantitation with sodium MR imaging—feasibility. *Radiology*. 2004;231:900-5.
  18. Insko EK, Kaufman JH, Leigh JS, Reddy R. Sodium NMR evaluation of articular cartilage degradation. *Magn Reson Med*. 1999;41:30-4.
  19. Nagarajan MB, Coan P, Huber MB, Diemoz PC, Glaser C, Wismuller A. Computer-aided diagnosis in phase contrast X-ray computed tomography for quantitative characterization of ex vivo human patellar cartilage. *IEEE Trans Biomed Eng*. 2013;60:2896-903.
  20. te Moller NC, Brommer H, Liukkonen J, Virén T, Timonen M, Puhakka PH, *et al*. Arthroscopic optical coherence tomography provides detailed information on articular cartilage lesions in horses. *Vet J*. 2013;197:589-95.
  21. Li X, Martin S, Pitris C, Ghanta R, Stamper DL, Harman M, *et al*. High-resolution optical coherence tomographic imaging of osteoarthritic cartilage during open knee surgery. *Arthritis Res Ther*. 2005;7:R318-23.
  22. Chu CR, Williams A, Tolliver D, Kwok CK, Bruno S 3rd, Irrgang JJ. Clinical optical coherence tomography of early articular cartilage degeneration in patients with degenerative meniscal tears. *Arthritis Rheum*. 2010;62:1412-20.
  23. Saied A, Cherin E, Gaucher H, Laugier P, Gillet P, Floquet J, *et al*. Assessment of articular cartilage and subchondral bone: subtle and progressive changes in experimental osteoarthritis using 50 MHz echography in vitro. *J Bone Miner Res*. 1997;12:1378-86.
  24. Kaleva E, Virén T, Saarakkala S, Sahlman J, Sirola J, Puhakka J, *et al*. Arthroscopic ultrasound assessment of articular cartilage in the human knee joint: a potential diagnostic method. *Cartilage*. 2011;2:246-53.
  25. Legare A, Garon M, Guardo R, Savard P, Poole AR, Buschmann MD. Detection and analysis of cartilage degeneration by spatially resolved streaming potentials. *J Orthop Res*. 2002;20:819-26.
  26. Préville AM, Lavigne P, Buschmann MD, Hardin J, Han Q, Djerroud L, *et al*. Electroarthrography: a novel method to assess articular cartilage and diagnose osteoarthritis by non-invasive measurement of load-induced electrical potentials at the surface of the knee. *Osteoarthritis Cartilage*. 2013;21:1731-7.
  27. Zipfel WR, Williams RM, Christie R, Nikitin AY, Hyman BT, Webb WW. Live tissue intrinsic emission microscopy using multiphoton-excited native fluorescence and second harmonic generation. *Proc Natl Acad Sci U S A*. 2003;100:7075-80.
  28. Centonze VE, White JG. Multiphoton excitation provides optical sections from deeper within scattering specimens than confocal imaging. *Biophys J*. 1998;75:2015-24.
  29. Chang G, Deniz CM, Honig S, Egol K, Regatte RR, Zhu Y, *et al*. MRI of the hip at 7T: feasibility of bone microarchitecture, high-resolution cartilage, and clinical imaging. *J Magn Reson Imaging*. 2014;39:1384-93.
  30. Banerjee S, Krug R, Carballido-Gamio J, Kelley DA, Xu D, Vigneron DB, *et al*. Rapid in vivo musculoskeletal MR with parallel imaging at 7T. *Magn Reson Med*. 2008;59:655-60.
  31. Gold GE, Thedens DR, Pauly JM, Fechner KP, Bergman G, Beaulieu CF, *et al*. MR imaging of articular cartilage of the knee: new methods using ultrashort TEs. *AJR Am J Roentgenol*. 1998;170:1223-6.
  32. Ramakrishnan P, Hecht BA, Pedersen DR, Lavery MR, Maynard J, Buckwalter JA, *et al*. Oxidant conditioning protects cartilage from mechanically induced damage. *J Orthop Res*. 2010;28:914-20.

33. Disler DG, McCauley TR, Wirth CR, Fuchs MD. Detection of knee hyaline cartilage defects using fat-suppressed three-dimensional spoiled gradient-echo MR imaging: comparison with standard MR imaging and correlation with arthroscopy. *AJR Am J Roentgenol.* 1995;165:377-82.
34. Recht MP, Piraino DW, Paletta GA, Schils JP, Belhobek GH. Accuracy of fat-suppressed three-dimensional spoiled gradient-echo FLASH MR imaging in the detection of patellofemoral articular cartilage abnormalities. *Radiology.* 1996;198:209-12.
35. Dupuy DE, Spillane RM, Rosol MS, Rosenthal DI, Palmer WE, Burke DW, et al. Quantification of articular cartilage in the knee with three-dimensional MR imaging. *Acad Radiol.* 1996;3:919-24.
36. Sittek H, Eckstein F, Gavazzeni A, Milz S, Kiefer B, Schulte E, et al. Assessment of normal patellar cartilage volume and thickness using MRI: an analysis of currently available pulse sequences. *Skeletal Radiol.* 1996;25:55-62.
37. Potter HG, Linklater JM, Allen AA, Hannafin JA, Haas SB. Magnetic resonance imaging of articular cartilage in the knee. An evaluation with use of fast-spin-echo imaging. *J Bone Joint Surg Am.* 1998;80:1276-84.
38. Roemer FW, Kwok CK, Hannon MJ, Crema MD, Moore CE, Jakicic JM, et al. Semiquantitative assessment of focal cartilage damage at 3T MRI: a comparative study of dual echo at steady state (DESS) and intermediate-weighted (IW) fat suppressed fast spin echo sequences. *Eur J Radiol.* 2011;80:e126-31.
39. Sonin AH, Pensy RA, Mulligan ME, Hatem S. Grading articular cartilage of the knee using fast spin-echo proton density-weighted MR imaging without fat suppression. *AJR Am J Roentgenol.* 2002;179:1159-66.
40. Yao L, Gentili A, Thomas A. Incidental magnetization transfer contrast in fast spin-echo imaging of cartilage. *J Magn Reson Imaging.* 1996;6:180-4.
41. Broderick LS, Turner DA, Renfrew DL, Schnitzer TJ, Huff JP, Harris C. Severity of articular cartilage abnormality in patients with osteoarthritis: evaluation with fast spin-echo MR vs arthroscopy. *AJR Am J Roentgenol.* 1994;162:99-103.
42. Cotofana S, Buck R, Dreher D, Wirth W, Roemer F, Duryea J, et al. Longitudinal (one-year) change in cartilage thickness in knees with early knee osteoarthritis: a within-person between-knee comparison. *Arthritis Care Res (Hoboken).* 2014;66:636-41.
43. Mintz DN, Hooper T, Connell D, Buly R, Padgett DE, Potter HG. Magnetic resonance imaging of the hip: detection of labral and chondral abnormalities using noncontrast imaging. *Arthroscopy.* 2005;21:385-93.
44. Li X, Kuo D, Theologis A, Carballido-Gamio J, Stehling C, Link TM, et al. Cartilage in anterior cruciate ligament-reconstructed knees: MR imaging T1 $\rho$  and T2—initial experience with 1-year follow-up. *Radiology.* 2011;258:505-14.
45. Stahl R, Luke A, Li X, Carballido-Gamio J, Ma CB, Majumdar S, et al. T1 $\rho$ , T2 and focal knee cartilage abnormalities in physically active and sedentary healthy subjects versus early OA patients—a 3.0-tesla MRI study. *Eur Radiol.* 2009;19:132-43.
46. Takayama Y, Hatakenaka M, Yoshiura T, Okazaki K, Nishikawa K, Okuaki T, et al. A simplified method of T(1) $\rho$  mapping in clinical assessment of knee joint. *Magn Reson Med Sci.* 2010;9:209-15.
47. Apprich S, Mamisch T, Welsch GH, Stelzener D, Albers C, Totzke U, et al. Quantitative T2 mapping of the patella at 3.0 T is sensitive to early cartilage degeneration, but also to loading of the knee. *Eur J Radiol.* 2012;81:e438-43.
48. Eshed I, Trattnig S, Sharon M, Arbel R, Nierenberg G, Konen E, et al. Assessment of cartilage repair after chondrocyte transplantation with a fibrin-hyaluronan matrix—correlation of morphological MRI, biochemical T2 mapping and clinical outcome. *Eur J Radiol.* 2012;81:1216-23.
49. Hirose J, Nishioka H, Nakamura E, Oniki Y, Yamashita Y, Mizuta H. T1 $\rho$  and T2 mapping of the proximal tibiofemoral joint in relation to aging and cartilage degeneration. *Eur J Radiol.* 2012;81:2776-82.
50. Li X, Benjamin Ma C, Link TM, Castillo DD, Blumenkrantz G, Lozano J, et al. In vivo T1 $\rho$  and T2 mapping of articular cartilage in osteoarthritis of the knee using 3 T MRI. *Osteoarthritis Cartilage.* 2007;15:789-97.
51. Plewes DB, Kucharczyk W. Physics of MRI: a primer. *J Magn Reson Imaging.* 2012;35:1038-54.
52. Matzat SJ, van Tiel J, Gold GE, Oei EH. Quantitative MRI techniques of cartilage composition. *Quant Imaging Med Surg.* 2013;3:162-74.
53. Nissi MJ, Töyräs J, Laasanen MS, Rieppo J, Saarakkala S, Lappalainen R, et al. Proteoglycan and collagen sensitive MRI evaluation of normal and degenerated articular cartilage. *J Orthop Res.* 2004;22:557-64.
54. Kelly BT, Potter HG, Deng XH, Pearle AD, Turner AS, Warren RF, et al. Meniscal allograft transplantation in the sheep knee: evaluation of chondroprotective effects. *Am J Sports Med.* 2006;34:1464-77.
55. Dunn TC, Lu Y, Jin H, Ries MD, Majumdar S. T2 relaxation time of cartilage at MR imaging: comparison with severity of knee osteoarthritis. *Radiology.* 2004;232:592-8.
56. Kim HK, Shiraj S, Anton CG, Horn PS, Dardzinski BJ. Age and sex dependency of cartilage T2 relaxation time mapping in MRI of children and adolescents. *AJR Am J Roentgenol.* 2014;202:626-32.
57. Mosher TJ, Dardzinski BJ, Smith MB. Human articular cartilage: influence of aging and early symptomatic degeneration on the spatial variation of T2—preliminary findings at 3 T. *Radiology.* 2000;214:259-66.
58. Surowiec RK, Lucas EP, Ho CP. Quantitative MRI in the evaluation of articular cartilage health: reproducibility and variability with a focus on T2 mapping. *Knee Surg Sports Traumatol Arthrosc.* 2014;22:1385-95.
59. Pachowsky ML, Trattnig S, Apprich S, Mauerer A, Zbyn S, Welsch GH. Impact of different coils on biochemical T2 and T2\* relaxation time mapping of articular patella cartilage. *Skeletal Radiol.* 2013;42:1565-72.
60. Wheaton AJ, Casey FL, Gougoutas AJ, Dodge GR, Borthakur A, Lonner JH, et al. Correlation of T1 $\rho$  with fixed charge density in cartilage. *J Magn Reson Imaging.* 2004;20:519-25.
61. Mosher TJ, Zhang Z, Reddy R, Boudhar S, Milestone BN, Morrison WB, et al. Knee articular cartilage damage in osteoarthritis: analysis of MR image biomarker reproducibility in ACRIN-PA 4001 multicenter trial. *Radiology.* 2011;258:832-42.
62. Takayama Y, Hatakenaka M, Tsushima H, Okazaki K, Yoshiura T, Yonezawa M, et al. T1 $\rho$  is superior to T2

- mapping for the evaluation of articular cartilage denaturalization with osteoarthritis: radiological-pathological correlation after total knee arthroplasty. *Eur J Radiol.* 2013;82:e192-8.
63. Klocke NF, Amendola A, Thedens DR, Williams GN, Luty CM, Martin JA, *et al.* Comparison of T1 $\rho$ , dGEMRIC, and quantitative T2 MRI in preoperative ACL rupture patients. *Acad Radiol.* 2013;20:99-107.
  64. Prasad AP, Nardo L, Schooler J, Joseph GB, Link TM. T1 $\rho$  and T2 relaxation times predict progression of knee osteoarthritis. *Osteoarthritis Cartilage.* 2013;21:69-76.
  65. Madelin G, Chang G, Otazo R, Jerschow A, Regatte RR. Compressed sensing sodium MRI of cartilage at 7T: preliminary study. *J Magn Reson.* 2012;214:360-5.
  66. Binks DA, Hodgson RJ, Ries ME, Foster RJ, Smye SW, McGonagle D, *et al.* Quantitative parametric MRI of articular cartilage: a review of progress and open challenges. *Br J Radiol.* 2013;86:20120163.
  67. Ward KM, Aletras AH, Balaban RS. A new class of contrast agents for MRI based on proton chemical exchange dependent saturation transfer (CEST). *J Magn Reson.* 2000;143:79-87.
  68. Wei W. Knee osteoarthritis: gagCEST MR imaging of articular cartilage (PhD dissertation). Columbus, OH: The Ohio State University; 2013.
  69. Singh A, Haris M, Cai K, Kassey VB, Kogan F, Reddy D, *et al.* Chemical exchange saturation transfer magnetic resonance imaging of human knee cartilage at 3 T and 7 T. *Magn Reson Med.* 2012;68:588-94.
  70. Potter HG, Black BR, Chong le R. New techniques in articular cartilage imaging. *Clin Sports Med.* 2009;28:77-94.
  71. Alexander AL, Lee JE, Lazar M, Field AS. Diffusion tensor imaging of the brain. *Neurotherapeutics.* 2007;4:316-29.
  72. Mlynárik V, Sulzbacher I, Bittšanský M, Fuiko R, Trattng S. Investigation of apparent diffusion constant as an indicator of early degenerative disease in articular cartilage. *J Magn Reson Imaging.* 2003;17:440-4.
  73. Raya JG, Dettmann E, Notohamiprodjo M, Krasnokutsky S, Abramson S, Glaser C. Feasibility of in vivo diffusion tensor imaging of articular cartilage with coverage of all cartilage regions. *Eur Radiol.* 2014;24:1700-6.
  74. Raya JG, Horng A, Dietrich O, Krasnokutsky S, Beltran LS, Storey P, *et al.* Articular cartilage: in vivo diffusion-tensor imaging. *Radiology.* 2012;262:550-9.
  75. Glaser C. New techniques for cartilage imaging: T2 relaxation time and diffusion-weighted MR imaging. *Radiol Clin North Am.* 2005;43:641-53.
  76. Zumstein V, Kraljević M, Conzen A, Hoechel S, Müller-Gerbl M. Thickness distribution of the glenohumeral joint cartilage: a quantitative study using computed tomography. *Surg Radiol Anat.* 2014;36:327-31.
  77. Hirvasniemi J, Kulmala K, Lammentausta E, Ojala R, Lehenkari P, Kamel A, *et al.* In vivo comparison of delayed gadolinium-enhanced MRI of cartilage and delayed quantitative CT arthrography in imaging of articular cartilage. *Osteoarthritis Cartilage.* 2013;21:434-42.
  78. Bansal P, Joshi N, Entezari V, Grinstaff M, Snyder B. Contrast enhanced computed tomography can predict the glycosaminoglycan content and biomechanical properties of articular cartilage. *Osteoarthritis Cartilage.* 2010;18:184-91.
  79. Bansal P, Stewart RC, Entezari V, Snyder BD, Grinstaff MW. Contrast agent electrostatic attraction rather than repulsion to glycosaminoglycans affords a greater contrast uptake ratio and improved quantitative CT imaging in cartilage. *Osteoarthritis Cartilage.* 2011;19:970-6.
  80. Silvast TS, Jurvelin JS, Aula AS, Lammi MJ, Töyräs J. Contrast agent-enhanced computed tomography of articular cartilage: association with tissue composition and properties. *Acta Radiol.* 2009;50:78-85.
  81. Kokkonen HT, Jurvelin JS, Tiitu V, Töyräs J. Detection of mechanical injury of articular cartilage using contrast enhanced computed tomography. *Osteoarthritis Cartilage.* 2011;19:295-301.
  82. Silvast TS, Kokkonen HT, Jurvelin JS, Quinn TM, Nieminen MT, Töyräs J. Diffusion and near-equilibrium distribution of MRI and CT contrast agents in articular cartilage. *Phys Med Biol.* 2009;54:6823-36.
  83. Batiste DL, Kirkley A, Laverty S, Thain LM, Spouge AR, Holdsworth DW. Ex vivo characterization of articular cartilage and bone lesions in a rabbit ACL transection model of osteoarthritis using MRI and micro-CT1. *Osteoarthritis Cartilage.* 2004;12:986-96.
  84. Wang G, Zhao S, Yu H, Miller CA, Abbas PJ, Gantz BJ, *et al.* Design, analysis and simulation for development of the first clinical micro-CT scanner. *Acad Radiol.* 2005;12:511-25.
  85. Chu CR, Lin D, Geisler JL, Chu CT, Fu FH, Pan Y. Arthroscopic microscopy of articular cartilage using optical coherence tomography. *Am J Sports Med.* 2004;32:699-709.
  86. Pan Y, Li Z, Xie T, Chu CR. Hand-held arthroscopic optical coherence tomography for in vivo high-resolution imaging of articular cartilage. *J Biomed Opt.* 2003;8:648-54.
  87. Saarakkala S, Wang SZ, Huang YP, Zheng YP. Quantification of the optical surface reflection and surface roughness of articular cartilage using optical coherence tomography. *Phys Med Biol.* 2009;54:6837-52.
  88. Huang YP, Saarakkala S, Toyras J, Wang LK, Jurvelin JS, Zheng YP. Effects of optical beam angle on quantitative optical coherence tomography (OCT) in normal and surface degenerated bovine articular cartilage. *Phys Med Biol.* 2011;56:491-509.
  89. Wang SZ, Huang YP, Wang Q, Zheng YP, He YH. Assessment of depth and degeneration dependences of articular cartilage refractive index using optical coherence tomography in vitro. *Connect Tissue Res.* 2010;51:36-47.
  90. Herrmann JM, Pitris C, Bouma BE, Boppart SA, Jesser CA, Stamper DL, *et al.* High resolution imaging of normal and osteoarthritic cartilage with optical coherence tomography. *J Rheumatol.* 1999;26:627-35.
  91. Hoffmeister BK, Wong AK, Verdonk ED, Wickline SA, Miller JG. Comparison of the anisotropy of apparent integrated ultrasonic backscatter from fixed human tendon and fixed human myocardium. *J Acoust Soc Am.* 1995;97:1307-13.
  92. O'Donnell M, Mimbs J, Miller J. Relationship between collagen and ultrasonic backscatter in myocardial tissue. *J Acoust Soc Am.* 1981;69:580-8.
  93. Pellaumail B, Watrin A, Loeuille D, Netter P, Berger G, Laugier P, *et al.* Effect of articular cartilage proteoglycan

- depletion on high frequency ultrasound backscatter. *Osteoarthritis Cartilage*. 2002;10:535-41.
94. Töyräs J, Rieppo J, Nieminen MT, Helminen HJ, Jurvelin JS. Characterization of enzymatically induced degradation of articular cartilage using high frequency ultrasound. *Phys Med Biol*. 1999;44:2723-33.
  95. Inkinen S, Liukkonen J, Ylärinne JH, Puhakka PH, Lammi MJ, Viren T, et al. Collagen and chondrocyte concentrations control ultrasound scattering in agarose scaffolds. *Ultrasound Med Biol*. 2014;40:2162-71.
  96. Huang YP, Zheng YP. Development of an arthroscopic ultrasound probe for assessment of articular cartilage degeneration. *Conf Proc IEEE Eng Med Biol Soc*. 2013;2013:144-7.
  97. Kim HK, Babyn PS, Harasiewicz KA, Gahunia HK, Pritzker KP, Foster FS. Imaging of immature articular cartilage using ultrasound backscatter microscopy at 50 MHz. *J Orthop Res*. 1995;13:963-70.
  98. Saarakkala S, Laasanen MS, Jurvelin JS, Töyräs J. Quantitative ultrasound imaging detects degenerative changes in articular cartilage surface and subchondral bone. *Phys Med Biol*. 2006;51:5333-46.
  99. Virén T, Saarakkala S, Kaleva E, Nieminen HJ, Jurvelin JS, Töyräs J. Minimally invasive ultrasound method for intra-articular diagnostics of cartilage degeneration. *Ultrasound Med Biol*. 2009;35:1546-54.
  100. Kaleva E, Toyraas J, Jurvelin JS, Virén T, Saarakkala S. Effects of ultrasound frequency, temporal sampling frequency, and spatial sampling step on the quantitative ultrasound parameters of articular cartilage. *IEEE Trans Ultrason Ferroelectr Freq Control*. 2009;56:1383-93.
  101. Saarakkala S, Töyräs J, Hirvonen J, Laasanen MS, Lappalainen R, Jurvelin JS. Ultrasonic quantitation of superficial degradation of articular cartilage. *Ultrasound Med Biol*. 2004;30:783-92.
  102. Spriet MP, Girard CA, Foster SF, Harasiewicz K, Holdsworth DW, Laverty S. Validation of a 40MHz B-scan ultrasound biomicroscope for the evaluation of osteoarthritis lesions in an animal model. *Osteoarthritis Cartilage*. 2005;13:171-9.
  103. Cherin E, Saied A, Pellaumail B, Loeuille D, Laugier P, Gillet P, et al. Assessment of rat articular cartilage maturation using 50-MHz quantitative ultrasonography. *Osteoarthritis Cartilage*. 2001;9:178-86.
  104. Disler DG, Raymond E, May DA, Wayne JS, McCauley TR. Articular cartilage defects: in vitro evaluation of accuracy and interobserver reliability for detection and grading with US. *Radiology*. 2000;215:846-51.
  105. Joiner GA, Bogoch ER, Pritzker KP, Buschmann MD, Chevrier A, Foster FS. High frequency acoustic parameters of human and bovine articular cartilage following experimentally-induced matrix degradation. *Ultrason Imaging*. 2001;23:106-16.
  106. Leicht S, Raum K. Acoustic impedance changes in cartilage and subchondral bone due to primary arthrosis. *Ultrasonics*. 2008;48:613-20.
  107. Wang L, Chen S, An KN, Yang HL, Luo ZP. Theoretical prediction of ultrasound elastography for detection of early osteoarthritis. *ScientificWorldJournal*. 2013;2013:565717.
  108. Morita Y, Kondo H, Tomita N, Suzuki S. A feasibility study for evaluation of mechanical properties of articular cartilage with a two-electrode electrical impedance method. *J Orthop Sci*. 2012;17:272-80.
  109. Frank EH, Grodzinsky AJ, Koob TJ, Eyre DR. Streaming potentials: a sensitive index of enzymatic degradation in articular cartilage. *J Orthop Res*. 1987;5:497-508.
  110. Changoor A, Coutu JP, Garon M, Quenneville E, Hurtig MB, Buschmann MD. Streaming potential-based arthroscopic device is sensitive to cartilage changes immediately post-impact in an equine cartilage injury model. *J Biomech Eng*. 2011;133:061005.
  111. Abedian R, Willbold E, Becher C, Hurschler C. In vitro electro-mechanical characterization of human knee articular cartilage of different degeneration levels: a comparison with ICRS and Mankin scores. *J Biomech*. 2013;46:1328-34.
  112. Novakofski KD, Williams RM, Fortier LA, Mohammed HO, Zipfel WR, Bonassar LJ. Identification of cartilage injury using quantitative multiphoton microscopy. *Osteoarthritis Cartilage*. 2014;22:355-62.
  113. Ross KA, Williams RM, Schnabel LV, Mohammed HO, Potter HG, Bradica G, et al. Comparison of three methods to quantify repair cartilage collagen orientation. *Cartilage*. 2013;4:111-20.
  114. Yeh AT, Hammer-Wilson MJ, Van Sickle DC, Benton HP, Zoumi A, Tromberg BJ, et al. Nonlinear optical microscopy of articular cartilage. *Osteoarthritis Cartilage*. 2005;13:345-52.
  115. Brockbank KG, MacLellan WR, Xie J, Hamm-Alvarez SF, Chen ZZ, Schenke-Layland K. Quantitative second harmonic generation imaging of cartilage damage. *Cell Tissue Bank*. 2008;9:299-307.
  116. Mansfield J, Yu J, Attenburrow D, Moger J, Tirlapur U, Urban J, et al. The elastin network: its relationship with collagen and cells in articular cartilage as visualized by multiphoton microscopy. *J Anat*. 2009;215:682-91.
  117. Williams RM, Zipfel WR, Tinsley ML, Farnum CE. Solute transport in growth plate cartilage: in vitro and in vivo. *Biophys J*. 2007;93:1039-50.
  118. Da Costa V, Wei R, Lim R, Sun CH, Brown JJ, Wong BJ. Nondestructive imaging of live human keloid and facial tissue using multiphoton microscopy. *Arch Facial Plast Surg*. 2008;10:38-43.
  119. Pavlova I, Hume KR, Yazinski SA, Peters RM, Weiss RS, Webb WW. Multiphoton microscopy as a diagnostic imaging modality for lung cancer. *Proc SPIE Int Soc Opt Eng*. 2010;7569:756918.
  120. Wang CC, Li FC, Wu RJ, Hovhannisyan VA, Lin WC, Lin SJ, et al. Differentiation of normal and cancerous lung tissues by multiphoton imaging. *J Biomed Opt*. 2009;14:044034.
  121. Skala MC, Squirrell JM, Vrotsos KM, Eickhoff JC, Gendron-Fitzpatrick A, Eliceiri KW, et al. Multiphoton microscopy of endogenous fluorescence differentiates normal, precancerous, and cancerous squamous epithelial tissues. *Cancer Res*. 2005;65:1180-6.